Wearable Disposable Electrotherapy

Mohamad FallahRad[1], Zeeshan Chaudhry[2], Mojtaba Belali Koochesfahani[1], Rayyan Bhuiyan[1], Mahdi Zaman[1], Tiffany Liu[1], Kisholoy Saha[1], Miguel R Diaz Uraga[1], Myesha Thahsin[1], Alexander Couzis[2], Marom Bikson[1]

1. Department of Biomedical Engineering, The City College of New York
2. Department of Chemical Engineering, The City College of New York

Abstract

We design and validate a novel electrotherapy platform, without any electronic components, using printed abundant environmentally-benign materials. Whereas existing electrotherapy devices use an independent power source and electronics to generate and control stimulation currents, our design eliminates the need for these components, reducing manufacturing complexity and costs. Our novel platform relies only on scalable manufacturing and environmentally-benign common materials. The disposable single-use platform is activated simply by placement on the body. A prescribed electrotherapy discharge is regulated by a novel electrochemical architecture. Production is scalable by relying only on additive manufacturing and low-cost materials, and tailored to any application in a flexible package (as discreet as adhesive bandages). The single-dose nature of this platform is a categorical shift from existing approaches with durable equipment that require programming and assembly to disposable electrodes for each use. Our Wearable Disposable Electrotherapy technology can be distributed like pharmacotherapy, with indications spanning neuromodulation of brain disorders, aesthetics, wound healing, transcutaneous drug delivery, and bioelectronic medicine.

Main

Applications of non-invasive electrical stimulation span treatment of pain and headache (1, 2), depression, addiction, age related cognitive decline (3, 4), wound healing (5, 6), aesthetic uses (7), bioelectronic medicine, and drug delivery (8). Electrical therapy devices have become compoundingly complex (microelectronics, stretchable electronics, wireless connectivity, etc.) (9, 6, 10). Battery-powered electronic devices must be connected to electrodes before each use, attached to the body, a discharge program initiated, and charged for subsequent use. The cost and cumbersomeness of electrical therapy contrasts with the “take and forget" usability of pharmaceuticals.

We develop the first electrotherapy platform that provides auto-initiated (upon application to the skin) controlled discharge in a single use, disposable, low-cost, conformable bandage. Enabling these features is an integrated printable design, absent any electronics (no circuit components) with power source, waveform control system, and interface elements made from environmentally-

benign common materials assembled layer by layer. The entire platform is thus printed on a common substrate, with an emergent 3D electrochemical architecture that is novel and enabling.

The Wearable Disposable Electrotherapy platform supports scalability and distribution models akin to pharmaceuticals. Each therapy-strip can be discreetly carried, applied in any environment, and disposed after use - just like an adhesive bandage. Indeed one application is accelerated wound healing. Addition of drugs with charged carriers to the skin interface allows a new class of transdermal drug-eluting therapy. Almost any existing application of non-invasive electrotherapy can be replaced.

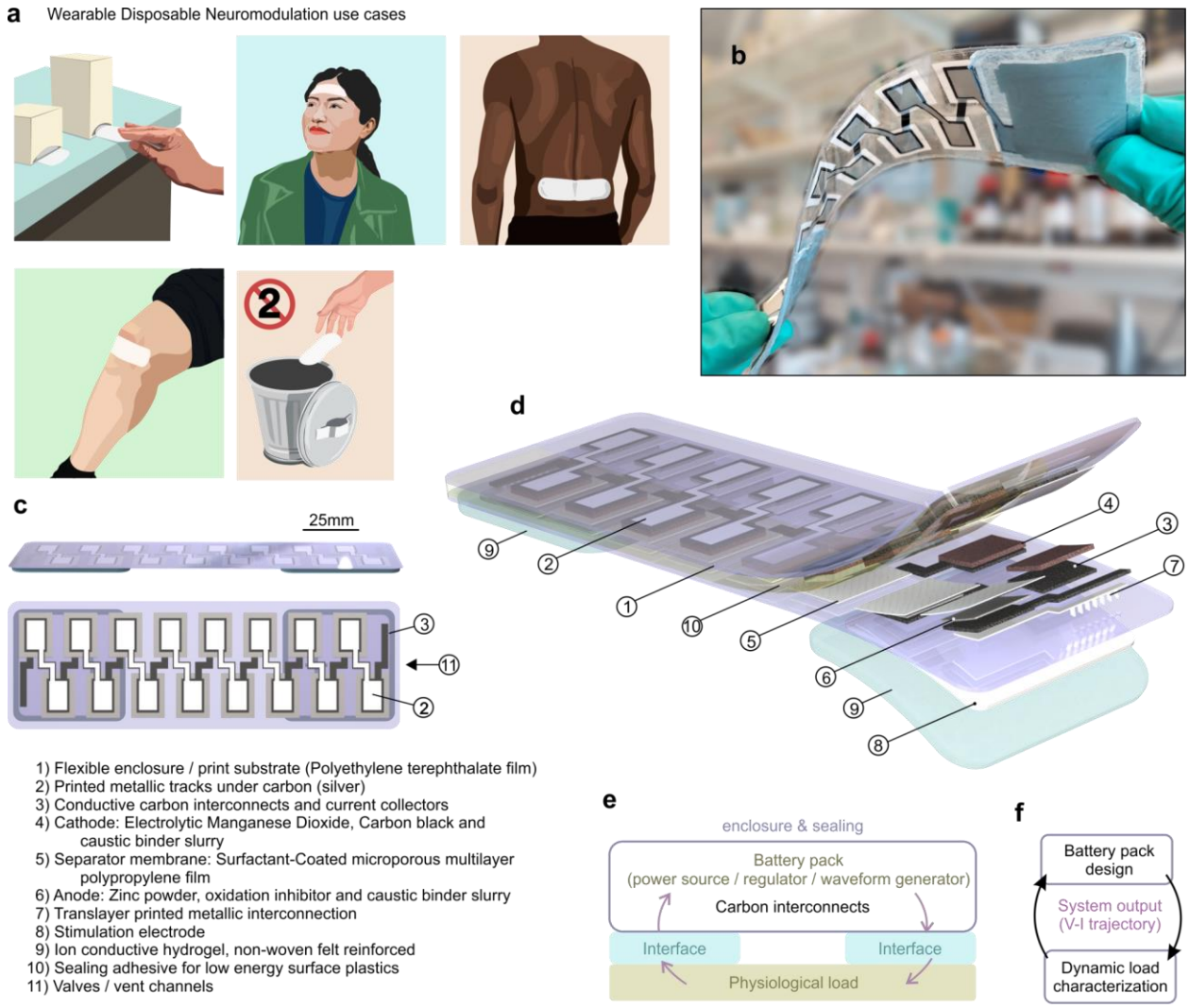

Fig. 1 | Wearable Disposable Electrotherapy device. **a)** Application-specific single-use devices are distributed and used akin to disposable bandages or pharmaceuticals. Applications include brain/cranial nerve stimulation (e.g. cognition, headache), electrical stimulation for pain, and accelerated wound healing. Devices are disposable as they are made without electronics and using environmentally-benign materials. **b)** Photograph of exemplary device. **c,d)** Device performance is enabled by a novel layered geometry of active materials and interfaces (element types 1-11), printed onto a common substrate (which becomes the device enclosure). **e)** System diagram: The device discharge is initiated and governed by interaction, through interface, with the target physiological load. Application-specific therapeutic dose (e.g. neuromodulation, transdermal drug delivery, bandage for wound healing) is thus controlled by the device shape and battery pack design. **f)** Unlike prior neuromodulation or battery technologies, discharge is neither current or voltage controlled. Device chemistry and architecture (battery packs) are designed based on dynamic load characteristics.

Results and Discussion

System design

Our goal is to develop a single-use disposable electrotherapy device that can compete in cost and usability with tablet pharmaceuticals. The novel design of the Wearable Disposable Electrotherapy platform addresses interdependent constraints spanning automatically initiated and controlled dosing, power density, packaging, and scalable manufacturing with only common, environmentally benign, and nonhazardous materials. The device design supports broad application-specific flexibility (dose, placement) (Fig. 1a).

1. The central innovation of this platform is avoidance of electronics (e.g. printed circuits, heavy metals) as electronics disallow a single-use (environmentally responsible disposable) device. The therapeutic dose is controlled through a printed structure using modular battery cells with interconnects. The battery pack structure, cell shape (tailoring areal energy density to thickness), active materials and mass inventory together provide the requisite voltage and dose control. Dose ramping is achieved through power-load interface design (internal battery pack resistance, electrodes, hydrogel thickness and ion mobility) and based on the progressive impedance changes associated with device application / removal.

2. The common substrate for the hydrogel and the power source removes any steps by the user ("no assembly required"). Devices are activated upon contact, where the body completes the device discharge circuit (Fig. 1e). Therefore to use the device, one needs only to apply it (e.g. absence of any controls, even a start button).

3. The platform is based entirely on additive fabrication and common/benign materials including active materials based on alkaline zinc/MnO_2 electrochemistry. Moreover, the battery does not require charging; it is fully activated during fabrication.

4. Packing, power, shape, and conformability design requirements are addressed using a novel multilayer planar battery cell pattern (Fig. 1c), created from 11 design elements (Fig. 1d), with a 3D structure fabricated entirely through additive fabrication. There is an overlay of electrochemical design (pack of battery cells connected by diagonal interconnects; Supplementary Fig. 1a), working-temperature regulation, mechanical design (including axes of bending with neutral surface on cells; Fig. 1b, Supplementary Fig. 1b), and sealing structures (including venting system; Supplementary 1d, Supplementary Fig. 3c).

Following these design features, the Wearable Disposable Electrotherapy devices may be distributed and used as cheaply and simply as pharmaceuticals. Our overall approach is thus orthogonal to efforts creating increasingly complex wearable electronics (9, 11, 12). The device performance is unlike prior electrical stimulation (strictly voltage or current controlled) or battery (limited discharge control) technologies, and rather requires a novel approach to dosing based on target waveform and dynamic device/physiological load (Fig. 1f).

Device structure

Given typical electrotherapy device voltages, required discharge rates, and duration (battery capacity) a stacked printed battery structure provides the required manufacturing flexibility. Disposable Wearable Electrotherapy device elements (Fig. 1c,d) include the electrochemical cells connected in series (13) in order to build up voltage and control discharge characteristics (Supplementary Fig. 1c), interconnects and interface elements (stimulation electrodes and hydrogel), and venting system. The design must integrate tunable discharge waveform, additive manufacturing and robust sealing, and high conformability.

Printed battery cells consistent of an associated anode and cathode, leading to corresponding cell terminals, are sealed to prevent electrolyte losses as well as to minimize cell-to-cell parasitic losses that result from electrolyte sharing between cells (Supplementary Fig. 2). The cells are connected in series (i.e cathode terminal from the previous cell is linked to the anode terminal of the following cell). The anode terminal of the first cell and the cathode terminal of the last cell in series comprise the terminals of the battery pack (power supply/control; Supplementary Figure 1c). These terminals are connected to the interface (Supplementary Fig. 1a,b), consisting of the stimulation electrode and hydrogel, which in turn provide connectivity to the body (Fig. 1e)

In order to fit the required number of cells in series within the physical constraints of the device area and supporting manufacturing, we have developed an innovative cell printing and packing approach. Anodes, cathodes, and their connections are printed in successive steps, in a symmetric geometric fashion on polyethylene terephthalate (PET) sheets. These sheets form the device enclosure. The interconnects between anodes and cathodes produce the required in-series connection between cells. In the final manufacturing step, the sheet is folded along its symmetry axis, marrying each anode element to its corresponding cathode element (of each cell), resulting in a fully functionalized battery pack (Supplementary Fig. 1a).

The device includes regions of relatively high flexural rigidity (battery cells) and axes of low flexural rigidity (Supplementary Fig. 1b). This mechanical design, that follows from the planer interlaced battery pack design, supports device conformability.

Interconnects are printed on both sides of the PET sheets; on the inner side (upon folding) connecting sequential batteries and on the outer side connecting battery pack terminals to the electrode of the interface (Supplementary Fig. 2; Supplementary Fig. 3). To further reduce interconnect resistance (from approximately 100 Ω for all interconnects to ~25 Ω), a thinner metal track is printed beneath the carbon conductive tracks. Printed carbon also passivates the metal track.

The Disposable Wearable Electrotherapy device (Fig. 1b,c,d, Supplementary Fig. 3) comprises of printable layers forming a battery pack (five layers), conductive interconnects (four layers), PET sheets enclosure (two layers), sealant (three layers), polypropylene (PP) strips to mask sealant as normally closed valves connecting inner space of batteries to vent channel, and ion conductive

hydrogels. The hydrogels serve as the interface between the device and the skin, facilitating electrical charge delivery and physical support of the device on skin. The positive and negative tabs of the battery pack are electrically connected to the stimulation electrodes via an array of micrometer-sized holes on the bottom substrate (Supplementary Fig. 3b). The 3D design results in a varied number of layers depending on position along device plane - from 3 at enclosure ends, to 9 over internal battery cells, to 11 at conductive hydrogels (not including vents and through holes) (Supplementary Fig. 2b and 3c).

The batteries adapt primary aqueous alkaline Zinc/Manganese Dioxide chemistry. Electrolytic Manganese Dioxide (EMD) is the cathode active material while metallic zinc is the active anode material. This chemistry offers safety, high energy density, and appropriate discharge rate. The anode and cathode are separated by a specialized membrane made from a porous PP film laminated to a non-woven PP, coated with a hydrophilic surfactant for aqueous applications. The membrane is suitable for extreme pH levels, and it maintains mechanical stability once wet. High device discharge rate is achieved by this high-porosity membrane, high surface area of each cell, low cell thickness, and high conductivity interconnects. Hydrogen gas generation (which can deform the enclosure) is lowered using a zinc alloy (with <100 ppm of indium and bismuth), and corrosion inhibitor additive to the alkaline electrolyte and is managed using a vent system (individual battery vents converging to one central channel of 1 mm width, Supplementary Fig. 2d, Supplementary Fig. 3c), which also supports effective vacuum sealing.

The exemplary Disposable Wearable Electrotherapy device is designed for low-intensity transdermal stimulation applications (7, 14) with a target dose of 3 ± 0.5 mA DC average over 20 ± 5 minutes (single-use ~150 mC/cm^2 capacity) in a conformable packaging with 2500 mm^2 interface electrodes (12 cm inter-electrode distance). A significant design aspect involves ensuring tolerability by limiting current transients at the initiation and end of stimulation (managed in conventional electrotherapy equipment with microcontrollers) and instantaneous peak current not to exceed 5.5 mA (controlled in electrotherapy equipment with feedback). Hydrogel electrodes are design for reliable current passage (>0.5 mm thick; volume resistivity of ~500 Ω.cm; (15), biocompatibility (ISO 10993-5, ISO 10993-10), and provide mechanical adhesion of the device to the skin (moderate skin pull-off adhesion, 20 - 50 g/cm; relative high adhesion on the device side, >100 g/cm), with no residue (e.g. felt reinforced) or irritation.

Scalable manufacture

The manufacturing process for Disposable Wearable Electrotherapy devices implements advanced methods that can be adapted for high-efficiency and high-volume (Fig. 2a). These processes are characterized by a combination of subtractive and additive approaches to produce an enabling 3D device structure (Fig. 2b, Supplementary Fig. 1a).

Fabrication commences with a precise laser-cutting of the PET sheet into specific geometries. To ensure a clean surface, a rinsing step using isopropyl alcohol is applied that targets the removal of any contaminants. Post rinsing, the PET sheet undergoes plasma treatment that alters the

surface energy of the sheet enhancing ink adhesion and ensuring effective sealing. This modified PET sheet becomes the foundation for deposition of the battery elements.

The battery elements are printed using inks that provide required functionalities. Metallic ink and carbon based ink with specific conductivity properties are used for all battery current collectors and interconnects among the battery cells. The initial phase involves the application of narrow metallic tracks, succeeded by broader carbon conductive interconnects; each printing stage is followed by drying and baking intervals to fix the features. The reason for this composite structure is improvement of resulting conductivity of interconnects (by ~75%). Following the printing of the conductive elements, the anode and cathode are deposited using designed active inks. The inks for the cathode comprise of 69 wt% EMD, 7 wt% graphite, 0.4 wt% acetylene black, 0.4 wt% silver oxide, 6 wt% KOH, 16 wt% deoxygenated DI water, and 1.2 wt% PVA. The inks for the anode comprise 75 wt% zinc powder, 0.4 wt% ZnO, 5 wt% KOH, 17.8 wt% deoxygenated DI water, 0.25 wt% PAA, and 1.55 wt% Na-CMC. The thickness of the anode and cathode materials, as dictated by design, is controlled by the use of screen / stencils. The cathode ink, post-application, undergoes a compaction process, which is necessary for low internal impedance of batteries.

Employing double-sided tape with an adhesive tailored for low surface energy polymer surfaces, the separator is assembled onto the substrate. The separator electrically isolates the anode and cathode active materials, preventing a short circuit, allowing only ionic transport. Our battery pack design includes a hydrogen management system for the gas generated during normal operation of aqueous batteries. Our gas management system comprises a channel that connects all the cells of the battery pack together permitting vent of generated gasses in each cell through a small pressure activated valve structure built into the adhesives used in the assembly of battery pack (Supplementary Fig. 2a,b and Fig. 3f).

The final manufacturing sequence involves the introduction of the electrolyte to the separator and the active materials, which results in an active, power-ready unit. The device is folded along the symmetry line of the inner surface (Supplementary Fig. 1a), sealed, and hydrogel is applied to the outer surface. Fig. 2c shows the resulting stack of different layers forming the device (at the hydrogel).

The structure of the battery electrodes and the film uniformity was confirmed by imaging using Scanning Electron Microscopy (SEM) of the deposited layers (Figure 2d). The separator membrane was also imaged using SEM to confirm the absence of defects that could result in short-circuiting a particular cell.

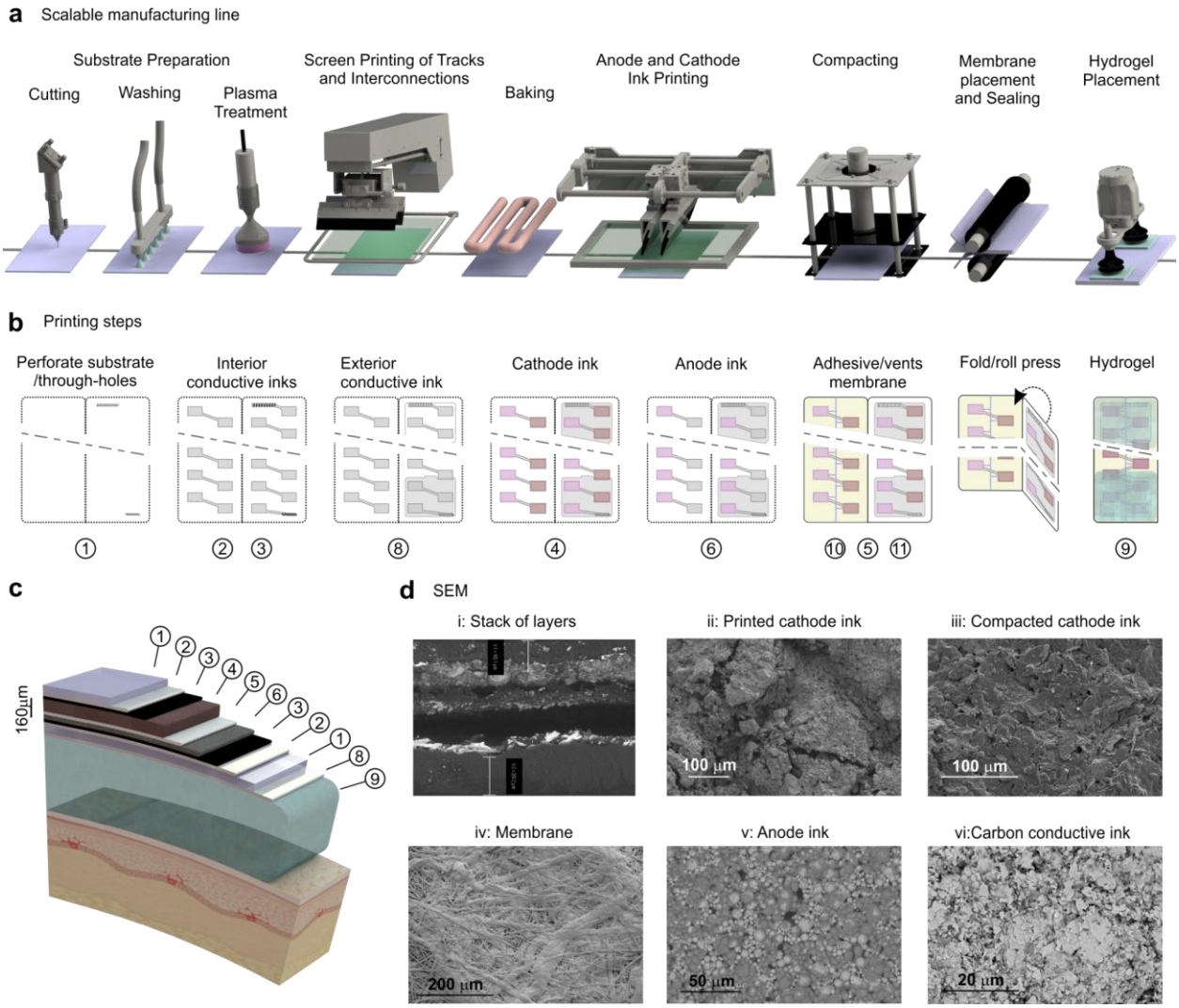

Fig. 2 I Wearable Disposable Electrotherapy manufacturing processes. **a**) Scalable manufacturing line consists of substrate preparation, printing interconnections, curing and baking, printing active materials, compacting, membrane placement and sealing and hydrogel placement. **b**) Steps of additive manufacturing on a single substrate leading to 3D device architecture. **c**) Schematic of layers forming the device including printed battery pack, interconnects, interface, and enclosure elements. **d**) SEM of i: device cross section ii: printed cathode ink iii: compacted cathode surface iv: printed anode ink v: two sides of membrane. Elements 1-11 labels as per Fig. 1.

Load Characterization

Unlike prior electrical stimulation devices that are current controlled or voltage controlled, Disposable Wearable Electrotherapy output is governed by the dynamic behavior of the battery pack, the interface (electrode, hydrogel), and the physiological load characteristics (Fig. 1f). For each application (target electrotherapy dose) the interface/physiological impedance must be characterized as part of Disposable Wearable Electrotherapy design.

A surrogate test device, devoid of battery pack material, connected at electrodes to a sourcemeter, was used to characterize interface and physiological impedance (Fig. 3a). Constant currents (with a 22.4 voltage limit) or constant voltages (with 6 mA current limit) were applied for 20 minutes (17 conditions across n=10 subjects). The surrogate test device was energized prior to application to the subjects' skin, to reproduce the application of Disposable Wearable Electrotherapy devices.

Under constant 3 mA stimulation, voltage gradually decreased in each subject (Fig. 3b). On average across subjects, voltage decreases gradually under 1-4 mA constant currents, but increases at ~14 min for 5-6 mA current (Fig. 3ci); these relationships are summarized in isotemporal lines (average load, Fig. 3cii; individual subjects' load, Supplementary Fig. 5) for subsequent battery pack design. The load impedance is dynamic as a function of applied current and time, reflecting nonlinear processes at the interface electrode (16) and skin (17, 18). Batteries do not provide constant current and their internal voltage/impedance is a nonlinear function of current draw; this creates a complex interdependence between source and load. Our novel battery pack design accounts for, and indeed leverages, interdependence by using the voltage presented by the load over time as a self-regulating mechanism of battery voltage.

Constant voltage stimulation (10-20 V) produces unreliable current (Fig. 3d). Current fluctuates on an experiment-wise basis over time. Current is not monotonic with time or applied voltage. These results confirm that voltage controlled stimulation (i.e. from an ideal battery) is not reliable for stimulation across interface and physiological loads. Our battery packs are designed to change in voltage with load.

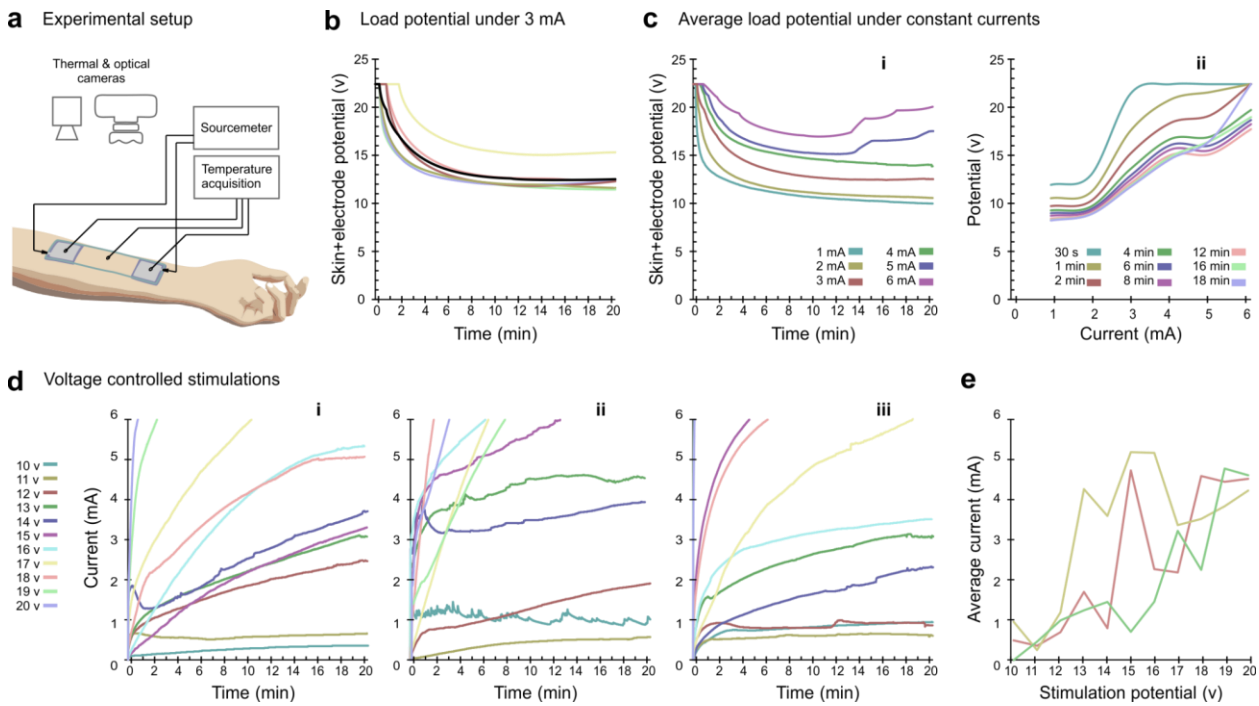

Fig. 3 I Load characterization for Wearable Disposable Electrotherapy device design. a) Experimental setup using the surrogate test device. **b)** Potential of load (skin+interface) under 3 mA over 20 minutes for individual subjects (colored lines) and average (black line). **c)** i: Average load potential over 20 minutes under constant currents (used to sizing of battery pack), associated ii: isotemporal V-I curves (used to simulate battery pack discharge). **d)** Voltage controlled stimulations over 20 minutes for three subjects (**i, ii, iii**) **e)** average current (over the active duration) by applied voltage. Note unreliable non-monotonic relationship for voltage controlled stimulation.

Battery pack design

Given the application specific target dose (3 mA, 20 minute) and associated load dynamics, an appropriate battery pack (power source with limited voltage and current) is designed. Provided system level parameters (ink formulation, screen thickness, separator type, electrolyte composition) and device structure (3D connectivity, fabrication / sealing technique) is established, our focus narrows to adjusting two dimensions to optimize battery performance: cell size and number of cells.

To this end, we conducted an array of single cell discharge tests, maintaining a consistent discharge rate of 3 mA over 30 minutes (Fig. 4a). During these tests, cell sizes ranged from 0.8 cm^2 to 2.4 cm^2, with constant areal densities of the active materials, and the resulting battery voltages were documented. We scaled these recorded voltages by factors ranging from 10 to 18. This provided us with projected battery pack voltages under a 3 mA discharge rate. Subsequently, we compared these values with the potential of the load (comprising the skin and electrodes) across a 20 minute stimulation period at a 3 mA amplitude (Fig 4bi). Our aim was to identify a battery size and the required number of cells that minimized the voltage variation throughout the 20 minute span and ensured the battery pack neither depleted prematurely nor persisted

substantially beyond the 20 minutes (Fig. 4bii). Following this analysis, a configuration of 1.5 cm^2 with 14 cells per pack was deemed optimal for the specified target dose.

The average potential of single 1.5 cm^2 cells over a 20-minute span across various discharge rates (1-6 mA); both average performance (Fig. 4ci, solid line) and performance variation due to variation in battery fabrication (Fig. 4ci, shaded) was measured (n = 72 cells). The average potential of the cells for up to a discharge depth of 1 mAh was calculated (Fig. 4cii).

We further characterized the performance of cells using potentiostatic electrochemical impedance spectroscopy (EIS) and developed an associated circuit analog model (Fig 4d). The lumped-parameter device impedance model reflects electrochemical processes occurring in the cell (19).

Verification and System Simulation

Having designed, for the target dose and load, the size and quantity of batteries for each pack, we fabricated and subjected these battery packs to galvanostatic discharge tests (n= 60 battery packs). The average potential of battery packs over a 20-minute span across various discharge rates (1-6 mA) was measured; both average performance (Fig. 4ei, solid line) and performance variation due to variation in battery fabrication (Fig. 4ei, shaded) is measured. The average potential of the battery packs for up to a discharge depth of 1 mAh was calculated (Fig. 4eii).

The battery pack discharge dynamics is represented in iso-temporal lines (colored dashed lines; Fig 4fi). These are overlaid with iso-temporal lines from the load average (colored solid line; Fig 4fi). For each time point, the interaction of these lines is represented (solid black line; Fig 4fi). The temporal evolution (over the stimulation duration) of the intersections between the voltage-current characteristics of the battery and of the load is the projected device output. This corresponds to the simulated Disposable Wearable Electrotherapy dosing for an average associated load. The projected output is then analyzed across multiple subjects, based on their respective load analysis (Supplementary Fig. 5; Fig 4fii). These trajectories show the projected operational envelope of the device (within a safe range). Reflecting our device design (chemistry and sizing), trajectories show the current will initially ramp up with limited decrease in voltage. As stimulation proceeds, the current reaches a maximum value after which the voltage decreases substantially limiting the delivery of current. A further decrease in voltage ramps current down.

As the device is thin and battery pack (polymer) elements are impacted by temperature, we quantified device heat dissipation (operational temperature). Sensors embedded in the device (over anode stimulation electrode, device center, and over cathode electrode) showed devices quickly (τ = 40 s) warm from room temperature to surface skin temperature (Supplementary Fig. 6a), with incrementally higher temperature at the cathode (Supplementary Fig. 6c, consistent with enhanced erythema). Associated warming at the skin surface was confirmed by thermal imaging Supplementary Fig. 6d. We further developed a computational model of device heat transfer (Supplementary Fig. 6a), consistent with experimental findings. These results confirm that primary heating reflects device warming to body surface temperature, consistent with conventional electrotherapies (20), during the initial (ramp up) period of discharge.

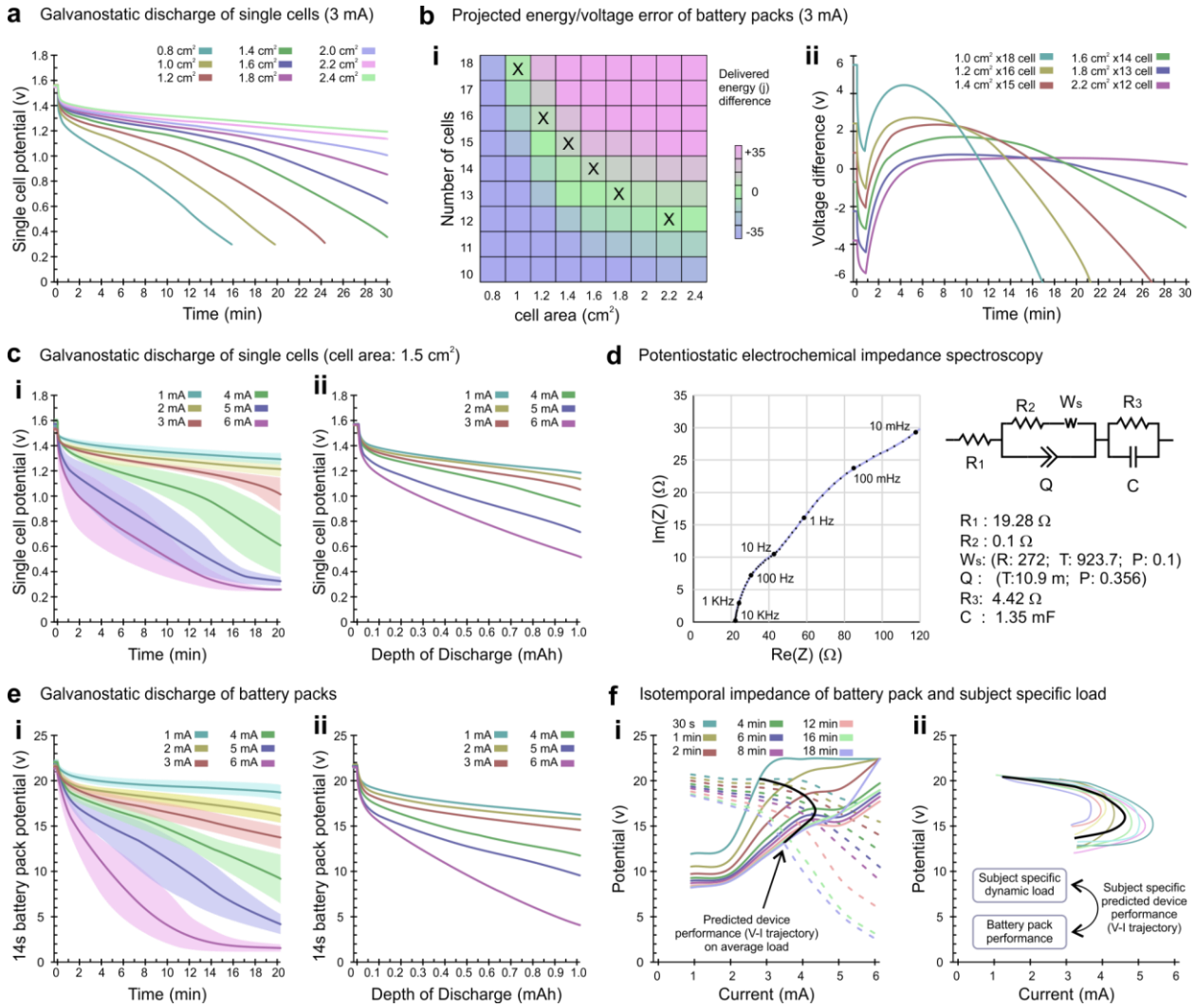

Fig. 4 | Design of Wearable Disposable Electrotherapy battery cell area and number (device sizing). **a)** Galvanostatic discharge curve of single cell batteries (average) with different cell sizes under 3 mA current over 30 minutes; **b i).** Projected energy (j) error of battery packs with 10 to 18 cells made from cells with different sizes under 3 mA discharge vs average of energy required to stimulate load with 3 mA during 20 minutes (x: selected designs for next stage); **b ii)** Voltage difference between six battery pack designs (selected based on minimal projected energy error) and voltage of load over 30 minutes at 3 mA. **c)** Galvanostatic discharge curve of single cells with sized area of 1.5 cm^2; **d)** Potentiostatic electrochemical impedance spectroscopy of single cell per 1 cm^2 area over frequency range of 10 mHz to 10 kHz with bias equal to OCV of freshly assembled battery and fitted model; **e)** Galvanostatic discharge curve of sized (14 cell, 1.5 cm^2 area) battery pack, **i**: over 20 minute time, **ii**: over discharge depth; **f i)** Isotemporal V-I curve of sized battery pack discharge (dashed lines) with overlaid average isotemporal V-I load curve (solid line). The intersection of these lines is the predicted discharge for the sized device into average load (black line). **f ii)** Given each subject's V-I load curve, a subject specific (colored lines) and average (black line) sized device discharge is simulated.

Validation

With chemistry and sizing designed for the exemplary application, Disposable Wearable Electrotherapy discharge performance was validated (n=10 subjects; Fig. 5a). Devices satisfied all other requirements, with a final thickness of 1.25 ± 0.07 mm and 10.5 ± 0.1 g. Devices were applied to the skin (t = 0) for 20 minutes and generated voltage (Fig. 5b) and current (Fig. 5c) measured. Across subjects voltage gradually decreased while current gradually increased (τ = 8.7 ± 3.4 min) to a peak (3.6 ± 0.8 mA) while current was sustained. A further decrease in voltage reduces current. Stimulation was sustained for the 20 minute application (average voltage 15.4 ± 2.4 V; average current 2.8 ± 0.7 mA; average power 41.8 ± 12 mW). As the device was removed the current was progressively aborted (τ = 5.0 ± 0.5 s).

Voltage-current trajectories (Fig. 5d) exemplify Disposable Wearable Electrotherapy dose control, and performance along system-design simulations (compare with Fig. 4fii). Discharge is neither strictly current-controlled or voltage-controlled, but for each subject is governed by battery-pack design given the dynamic impedance response. Load impedance initially decreased with current application (Fig. 5e), but reliably plateaued and normalized across subjects (range 4-7 kΩ at 18 minutes).

Discomfort during electrotherapy was assessed by conventional VAS rating (15) at 11 timepoints during stimulation. Stimulation was well tolerated (average pain VAS 1.1 ± 0.75; across 110 measurements never >3; Figure 5g), with expected transient erythema, and no lasting skin irritation. Subject's transient and mild perceptions of current flow (e.g. "tingling") are consistent with functional electrical delivery (i.e. activation of nerves; 21).

Uniformity of current delivery was assessed at the electrodes and at the skin. Charge uniformity was imaged (pre/post discharge, 2D optical scan) at the anode electrode, as evidenced by oxidation, and at the cathode electrode, as evidenced by gas evolution (Fig. 5h). Average normalized charge density was uniform at the cathode and moderately higher at electrode edges (annular) at the anode. Stimulation uniformity at the skin was accessed by high-resolution photography (pre/post discharge) of skin erythema (Figure 5i; 22). Immediately post-discharge, erythema was relatively uniform under the cathode, while milder and punctate under the anode. At appropriate doses, erythema is expected and transient (22), non-hazardous and consistent with skin stimulation, and - in the context of iontophoretic drug delivery and wound healing - desired (5, 21).

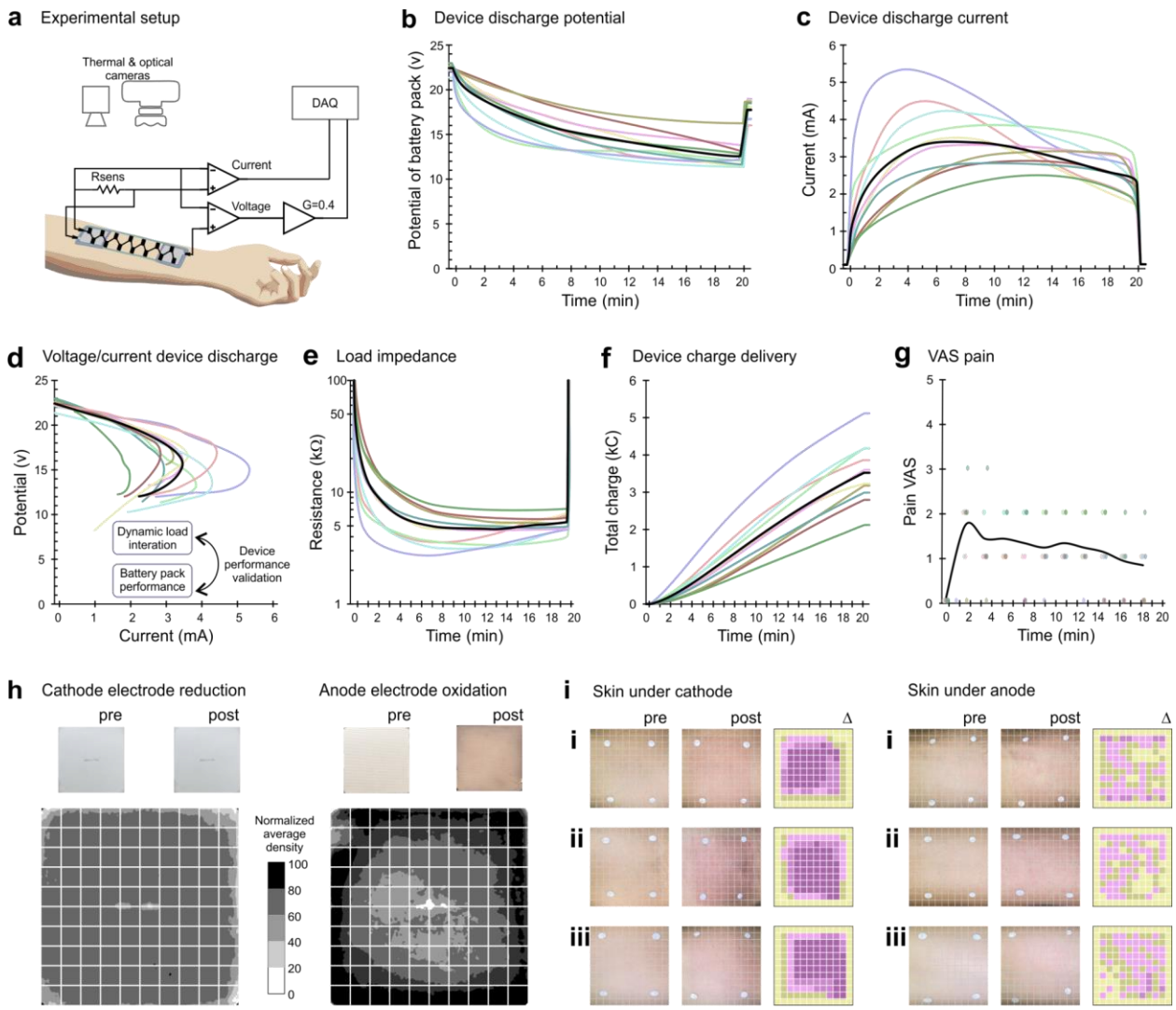

Fig 5 | Validation of Wearable Disposable Electrotherapy self-regulated discharge. **a)** Experimental setup for the target application across subjects' forearms. Individual subjects (colored lines) and average (black) lines are shown. **b)** Voltage of battery packs and **c)** output current over 20 minutes of stimulation. **d)** V-I curve of device throughout the stimulation. Compare these measured discharges with device-design simulation (Fig 5fii). **e)** Impedance of the load (electrodes + skin), **f)** cumulative charge delivered across the load, and **g)** pain levels over the 20 minutes of stimulation. **h)** Distribution of cathode electrode reduction and anode electrode oxidation. **i)** Skin redness relative heat map under cathode electrode and under anode electrode, for three subjects (**i, ii, iii**).

Conclusions

In summary we designed, fabricated, and validated the first electrotherapy platform using additive manufacturing with common environmentally-benign materials - without electronics.
Device packing, power, shape, and conformability design requirements are addressed using this multilayer battery cell pattern. Electrotherapy dose is “built into " device architecture/chemistry, with discharge initiated simply by applying the device. We develop an associated theoretical framework for device design based on coupling between load and battery pack. Platform manufacture can be scaled and customized with printable circuit technologies (23), non-linear conductive polymers, and printable sensor-like materials (e.g. sensitive to temperature, humidity, pressure).

Wearable Disposable Electrotherapy can be distributed like drugs, as dose / indication specific adhesive strips (Fig 1a). A patient can carry a single device (e.g. folded in a pocket), simply apply it discreetly when needed, and then discard the device. Based on iontophoretic drug delivery or stimulation erythema, drug alluding strips are thus made practical. The established principle of electrical wound healing can be made practical with disposable electrically driven bandages. Head applied strips can provide neuro-psychiatric therapies based on cranial nerve stimulation or cortex stimulation. This paper serves to show these and other applications are technically feasible. This paper thus established the principles of a new field of electrotherapy, one that can blur the line with pharmacotherapy.

References

1. Vance, Carol GT, et al. "Using TENS for pain control: the state of the evidence." Pain management 4.3 (2014): 197-209.
2. Coppola, Gianluca, et al. "Neuromodulation for chronic daily headache." Current Pain and Headache Reports 26.3 (2022): 267-278.
3. Fregni, Felipe, et al. "Evidence-based guidelines and secondary meta-analysis for the use of transcranial direct current stimulation in neurological and psychiatric disorders." International Journal of Neuropsychopharmacology 24.4 (2021): 256-313.
4. Antal, Andrea, et al. "Low intensity transcranial electric stimulation: safety, ethical, legal regulatory and application guidelines." Clinical neurophysiology 128.9 (2017): 1774-1809.
5. Thakral, Gaurav, et al. "Electrical stimulation to accelerate wound healing." Diabetic foot & ankle 4.1 (2013): 22081.
6. Jiang, Yuanwen, et al. "Wireless, closed-loop, smart bandage with integrated sensors and stimulators for advanced wound care and accelerated healing." Nature Biotechnology 41.5 (2023): 652-662.
7. Bikson, Marom, et al. "Limited output transcranial electrical stimulation (LOTES-2017): Engineering principles, regulatory statutes, and industry standards for wellness, over-the-counter, or prescription devices with low risk." Brain stimulation 11.1 (2018): 134-157.
8. Karpiński, Tomasz M. "Selected medicines used in iontophoresis." Pharmaceutics 10.4 (2018): 204.
9. Wang, Weichen, et al. "Neuromorphic sensorimotor loop embodied by monolithically integrated, low-voltage, soft e-skin." Science 380.6646 (2023): 735-742.
10. Jiang, Min, et al. "Advances in smart sensing and medical electronics by self-powered sensors based on triboelectric nanogenerators." Micromachines 12.6 (2021): 698.
11. Ye, Cui, et al. "A wearable aptamer nanobiosensor for non-invasive female hormone monitoring." Nature Nanotechnology (2023): 1-8.
12. Xu, Gang, et al. "Battery-free and wireless smart wound dressing for wound infection monitoring and electrically controlled on-demand drug delivery." Advanced Functional Materials 31.26 (2021): 2100852.
13. Gaikwad, Abhinav M., et al. "A flexible high potential printed battery for powering printed electronics." Applied Physics Letters 102.23 (2013).
14. Paneri, Bhaskar, et al. "Tolerability of repeated application of transcranial electrical stimulation with limited outputs to healthy subjects." Brain Stimulation 9.5 (2016): 740-754.

15. Khadka, Niranjan, et al. "Dry tDCS: Tolerability of a novel multilayer hydrogel composite non-adhesive electrode for transcranial direct current stimulation." Brain stimulation 11.5 (2018): 1044-1053.
16. Merrill, Daniel R., Marom Bikson, and John GR Jefferys. "Electrical stimulation of excitable tissue: design of efficacious and safe protocols." Journal of neuroscience methods 141.2 (2005): 171-198.
17. Bora, Dhruba Jyoti, and Rajdeep Dasgupta. "Estimation of skin impedance models with experimental data and a proposed model for human skin impedance." IET Systems Biology 14.5 (2020): 230-240.
18. Unal, Gozde, et al. "Quasi-static pipeline in electroconvulsive therapy computational modeling." Brain Stimulation 16.2 (2023): 607-618.
19. Lazanas, Alexandros Ch, and Mamas I. Prodromidis. "Electrochemical Impedance Spectroscopy— A Tutorial." ACS Measurement Science Au (2023).
20. Khadka, Niranjan, et al. "Minimal heating at the skin surface during transcranial direct current stimulation." Neuromodulation: Technology at the Neural Interface 21.4 (2018): 334-339.
21. Xu, Xinkai, et al. "Effects of electrical stimulation on skin surface." Acta Mechanica Sinica (2021): 1-29.
22. Ezquerro, Fernando, et al. "The influence of skin redness on blinding in transcranial direct current stimulation studies: a crossover trial." Neuromodulation: Technology at the Neural Interface 20.3 (2017): 248-255.
23. Sousa, Ricardo E., Carlos M. Costa, and Senentxu Lanceros-Méndez. "Advances and future challenges in printed batteries." ChemSusChem 8.21 (2015): 3539-3555.
24. Guleyupoglu, Berkan, et al. "Reduced discomfort during high-definition transcutaneous stimulation using 6% benzocaine." Frontiers in neuroengineering 7 (2014): 28.
25. Minhas, Preet, et al. "Electrodes for high-definition transcutaneous DC stimulation for applications in drug delivery and electrotherapy, including tDCS." Journal of neuroscience methods 190.2 (2010): 188-197.
26. Zannou, Adantchede L., Niranjan Khadka, and Marom Bikson. "Bioheat Model of Spinal Column Heating During High-Density Spinal Cord Stimulation." Neuromodulation: Technology at the Neural Interface 26.7 (2023): 1362-1370.
27. Datta, Abhishek, Maged Elwassif, and Marom Bikson. "Bio-heat transfer model of transcranial DC stimulation: comparison of conventional pad versus ring electrode." 2009 Annual International Conference of the IEEE Engineering in Medicine and Biology Society. IEEE, 2009.

Methods

Manufacture.

Substrate preparation. The substrate is fabricated from 100 µm-thick PET sheets (McMaster #8567K44) which undergo a series of preparation steps: 1) Heat treating of the substrate for the purpose of mechanical stability by baking at 90°C for 15 minutes; 2) Laser cutting to perforate boundaries of the device and folding line as well as throughholes. This allows the pouch to be a part of the substrate sheet during printing steps, and subsequently to be separated for sealing of the battery pouch. The fold line facilitates accurate alignment of battery electrodes during folding while preventing easy tearing; 3) Washing with isopropyl alcohol followed by air drying; 4) Surface treatment with cold plasma (Relyon plasma piezo brush PZ3) to improve adhesion.

Printing of conductive tracks (interconnect, through holes, stimulation electrodes, current collectors). A silver conductive ink (Saral Silver 700) is screen printed (Novastar SPR-45 stencil/screen printer) onto both sides of the substrate (Supplementary Fig. 2a and 2c). Following printing, the substrate is heated in an oven (90C) to facilitate the evaporation of the solvents present in the ink used. After baking, the thickness of the printed silver track is ~20 µm. Subsequently, a carbon passivation layer (Saral Carbon 700A) is screen printed and baked in a similar fashion; this was only on the inner side with a screen template 1 mm wider than that used for silver from each side. After baking, the thickness of the printed carbon track is ~40 µm.

To establish an electrical connection between both sides of the substrate, we implement laser-cutting to create micrometer-sized holes in the form of an array in the substrate before printing.

During the screen printing of the conductive inks on both sides of the substrate, the ink permeates these holes, creating a conductive path between the two sides of the substrate. The size and number of these holes are tailored to specific ink properties (rheology and particle size) to achieve reliable adhesion and conductivity. To support device verification and validation, three conductive tabs were added to the design at the battery pack terminals and at the cathode stimulation electrode, which allow monitoring of current and voltage.

Preparation of cathode ink, anode ink and electrolyte. The cathode ink is composed of 70 wt% electrolytic manganese dioxide (EMD), 3.5 wt% carbon black as a conductive additive, 5 wt% KOH, 20 wt% deoxygenated DDI water, and 1.5 wt% PVA (average MW 94k) as a binder. The slurry is prepared by mixing water and PVA and KOH in a nitrogen box to prevent oxygen dissolution in water during mixing. This solution then is sealed and kept in the refrigerator at 4 °c. Prior to use, the mix of EMD powder and carbon black powder is added and mixed and finally loaded into a syringe for application.

The anode ink consists of 75 wt% zinc powder, 0.4 wt% zinc oxide as corrosion inhibitor, 5 wt% KOH, 17.8 wt% deoxygenated DDI water, 0.25 wt% PAA (average MW 450k), and 1.55 wt% Na-CMC (average MW 90k) as binders. The slurry is prepared by mixing all ingredients, except for zinc powder, in a nitrogen box to prevent oxygen dissolution. The slurry is then sealed and refrigerated at 4 °c. Prior to use, zinc powder is added to the solution inside of a syringe and mixed to create the anode ink.

The electrolyte is formulated with 75 wt% deoxygenated DDI water and 25 wt% KOH.

Sealing method. The device is sealed using a double-sided acrylic adhesive designed for low surface energy plastics, with an interior carrier film for enhanced mechanical stability With a thickness (0.17 mm) less than the battery pack cells and interconnects (3M 9495LE). The double-sided adhesive sheet is cut (prior to removing the liner of both sides) using a laser cutter into two strips, each with openings corresponding to cells on one row of the battery pack (Supplementary Fig. 3f). When placed on the substrate a gap between the two adhesive strips forms the central channel of the venting system (Supplementary Fig. 2d and 3f).

Placement of separator. The separator membrane (Celgard 5550) used consists of polypropylene film laminated to a polypropylene nonwoven fabric, coated with hydrophilic surfactant for aqueous applications. This membrane has a thickness of 110 µm and 55% porosity, for high electrolyte retention and ion conductivity for high discharge rate. The membrane is laser cut to appropriate size and placed on the cell using cut double sided tape.

Vent channel and valves. After placing the membranes on double sided tape, thin (10 µm) strips of PP (1 mm width) are placed on the adhesive, connecting the middle of the battery cell to the vent channel (Supplementary Fig. 2d and 3c). These thin strips mask the adhesive, creating normally closed valves, they provide an escape for air (during battery pack sealing) or generated hydrogen by the cells, to the vent channel.

Printing of active materials on current collectors. Each membrane is saturated with 9.5 mg (8 µL) of electrolyte before printing active materials. The volume of electrolyte is crucial to control since insufficient electrolyte reduces battery performance, while excess electrolyte wets the surface of double sided tape resulting in poor sealing. Then anode and cathode inks are deposited on printed substrates using screen / stencil. Immediately after printing anode ink, double sided tapes with soaked membranes are placed on two anode rows of the device. This prevents printed zinc from drying. By folding the device on its fold line, both sides of the substrate meet in alignment to form a sealed battery pack (Supplementary Fig. 2a). The sealed battery pack goes through a roller from each side to the middle of the device where the vent channel is to push trapped air out of cells through valves.

Battery pack quality control. After compressing the pack, terminals of the pack are connected to a multimeter to read the initial open circuit voltage (IOCV). Some manufacturing problems can be detected by observing subtle changes of voltage.

Interface hydrogel application. Ion conductive hydrogels (Axelgaard AG625) are cut to the size (45 mm x 56 mm, 25.2 cm^2) and placed on the stimulation electrodes. As needed, fastening (non-conductive) hydrogel (Axelgaard AG535) can be used in between stimulation electrodes. The hydrogels are covered with PET liner until use. The hydrogel placement step was omitted for battery pack discharge verification tests. The optimization of hydrogel (and associated stimulation electrode material) for the exemplary application followed protocols developed in our lab (14, 15, 24, 25) screening for a) tolerability; b) skin irritation; c) impedance (compliance voltage); and d) material/mechanical properties.

Device Verification.

Electrical performance verification of cell / battery packs under constant current discharge was conducted using a sourcemeter (Keithley 2450 SMU). Electrochemical impedance spectroscopy (EIS) experiments were conducted with a Prinston Applied VersaSTAT 4 Potentiostat/Galvanostat. AC impedance measurements were performed potentiostatically at open circuit voltage and a small signal stimulus of 5 mV within a frequency range of 10 mHz - 10 kHz. The test is conducted with 60 data points distributed across the frequency range on a logarithmic scale. The battery model components were selected based on comparable electrochemistry analysis (19) and fit to EIS data (AMETEK, ZView). Model parameters reflect mass transfer, chemical kinetics, and electrical resistance of current collectors and conductive additives in electrodes, from which device chemistry (particle size, electrode porosity) and structure (thickness of electrode, compaction) can be refined. This includes the upper limit on current density limited by mass transfer of charge carriers. SEM images recorded using SUPRA 55, with an acceleration voltage of 16 kV and backscattered electron detector.

Load Characterization and Validation.

Participants. The study was conducted in accordance to protocols and procedures approved by the Institutional Review Board of the City College of New York. All volunteer participants provided written informed consent to participate in the study. The study included 10 subjects (8 male)

between the ages of 19 and 37 (M = 26, SD = ±6.5). All subjects were recruited through local advertisement and financially compensated.

Screening and exclusion criteria. Participants were excluded if they presented with any skin disorder at or near stimulation locations that compromised skin integrity, such as eczema, rashes, blisters, open wounds, burns including sunburns, cuts, or other skin defects, as the goal of this study was not to determine if skin impairments influence the tolerability or to access electrical stimulation to enhance wound healing.

Stimulation were applied to the ventral or dorsal side of the subject's left or right forearm. No more than one dose was applied to a region per day (e.g. ventral surface of right arm). All devices were at room temperature (22 °c) immediately prior to testing.

Load characterization. For load characterization tests, surrogate test devices with the same design as Wearable Disposable Electrotherapy but without deposition of active materials were made. Prior to the test, subjects' forearms were cleansed with soap and water and then dried. After placement of ion conductive hydrogels the monitoring tabs were connected to a sourcemeter (Keithley 2450 SMU). According to the test, the sourcemeter output was set to either constant voltage (10-20 v) limit of 6mA, or to constant current (1-6 mA) with limit of 22.4 v. Output was enabled before placement of the test device on skin.

Temperature was recorded using three thermocouple probes placed in the empty battery pouch, one over the anode stimulation electrode, one over the cathode stimulation electrode and one in the middle of the device over fastening hydrogel. Photographs were taken immediately before and after stimulation under consistent lighting conditions and skin temperature was recorded using a thermal camera (FLIR One Pro). At the beginning and during stimulation, subjects reported subjective pain on a VAS scale every 2 minutes. Approximately 24 hours after stimulation, subjects' skin was evaluated for any enduring skin irritation.

Validation. The procedure was similar to load tests using the surrogate test device; instead of connecting the device to the sourcemeter, the Wearable Disposable Electrotherapy Device with active batteries was used. To record the voltage and current of the device, a custom high impedance analog interface was used (0.4 attention factor), a 100 Ω series resistor (for current), and acquisition system (DATAQ DI-1100).

FEM Device Stimulation.

We developed a computer-aided design (CAD) model of the Wearable Disposable Electrotherapy prototype and underlying superficial tissue. The biophysical and thermo-electrical properties of biological tissues were based on previous studies and heat-transfer biophysics followed standard assumptions and methods (26, 27). An approximate temperature distribution throughout a perfused tissue can be found by solving the bio-heat transfer (Pennes) equation. For the thermal boundary conditions, all external boundaries were insulated except the top surface which was assigned heat flux. Structures were modeled as CAD files in SolidWorks (Dassault Systemes

Corp., MA, USA) and imported and computationally solved in COMSOL (COMSOL Multiphysics, Boston, MA). The resulting finite element model comprised >5,000,000 tetrahedral elements (>54,000,000 degrees of freedom) with 10 s time-steps.

Supplementary data

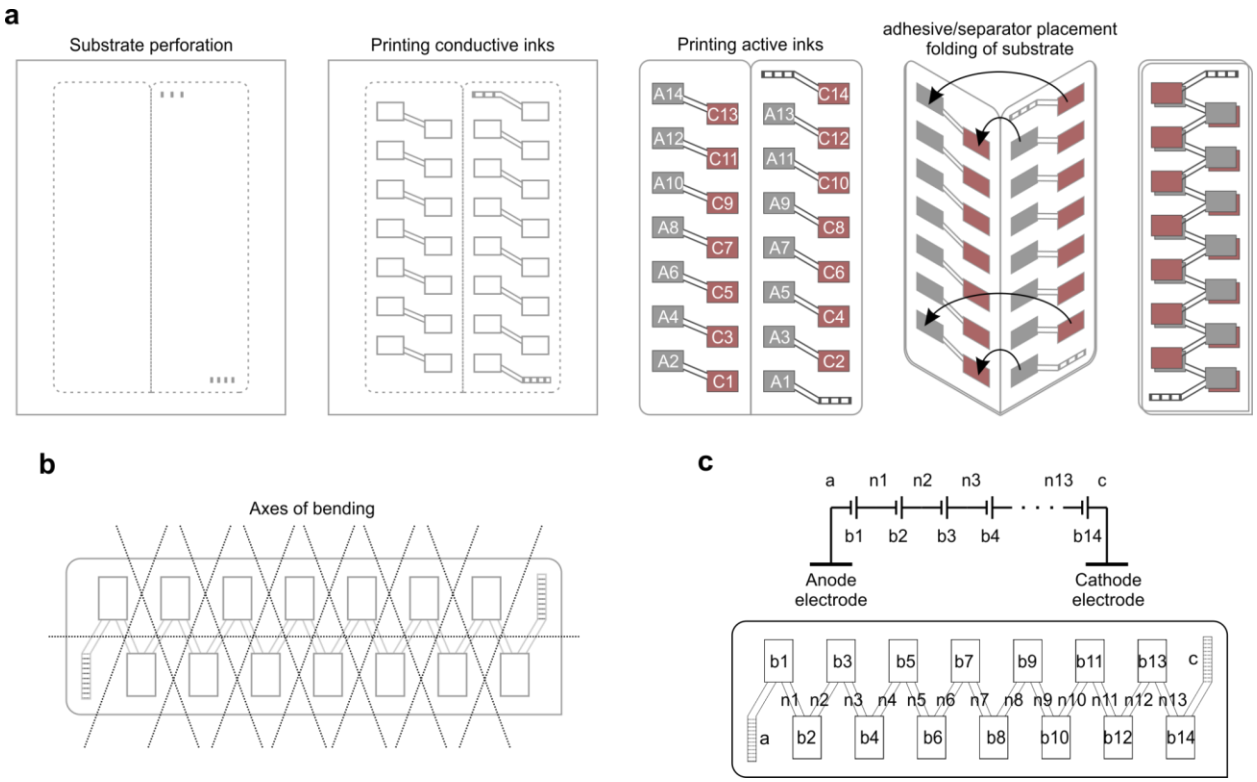

Supplementary Fig. 1. Formation of 3D structure and battery pack functionality of Wearable Disposable Electrotherapy device. **a)** All components, including interconnect and active materials (forming cell pairs, numbered), are printed on a single substrate. In the final manufacturing steps separators and adhesive are added and the device folded, whereby battery cells are formed and connected. **b)** The geometry further supports conformability along 14 low flexural rigidity axes. **c)** The battery pack output at the terminals (a: stimulation anode, c: stimulation cathode) reflects the series output of battery cells (b1 to b14) through interconnects (n1 to n13).

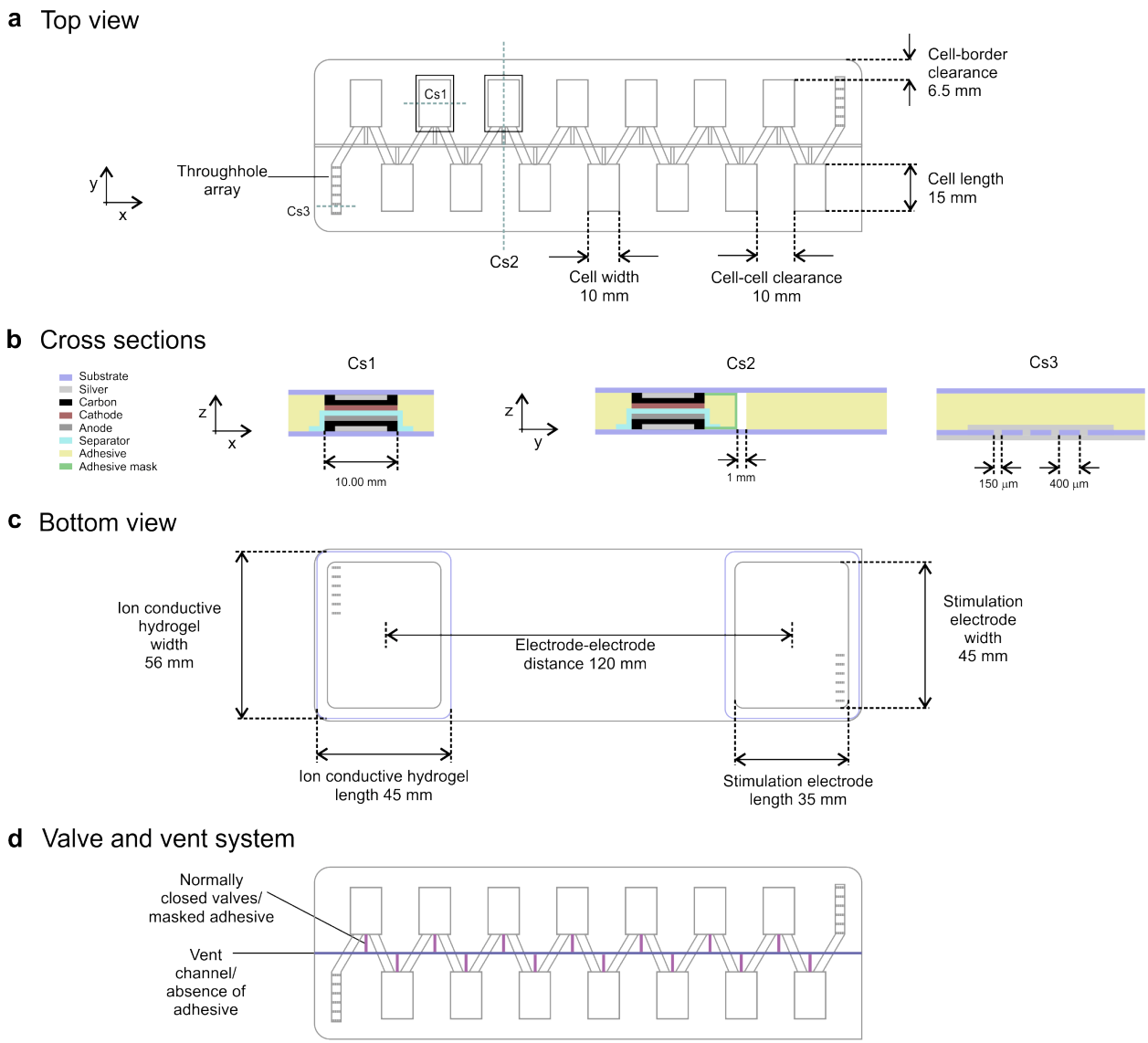

Supplementary Fig. 2. Geometry of Wearable Disposable Electrotherapy device (battery pack structure and interconnects, interfaces, venting system). **a)** Device top view showing electrochemical architecture of series cells leading to battery pack terminals (with interconnects to bottom substrate), and integrated venting system. **b)** Device cross sections at battery cell, throughholes and middle of device showing masked adhesive and vent channel. **c)** Device bottom view showing interface components with throughhole interconnects to top substrate. **d)** Device cross section highlighting venting system.

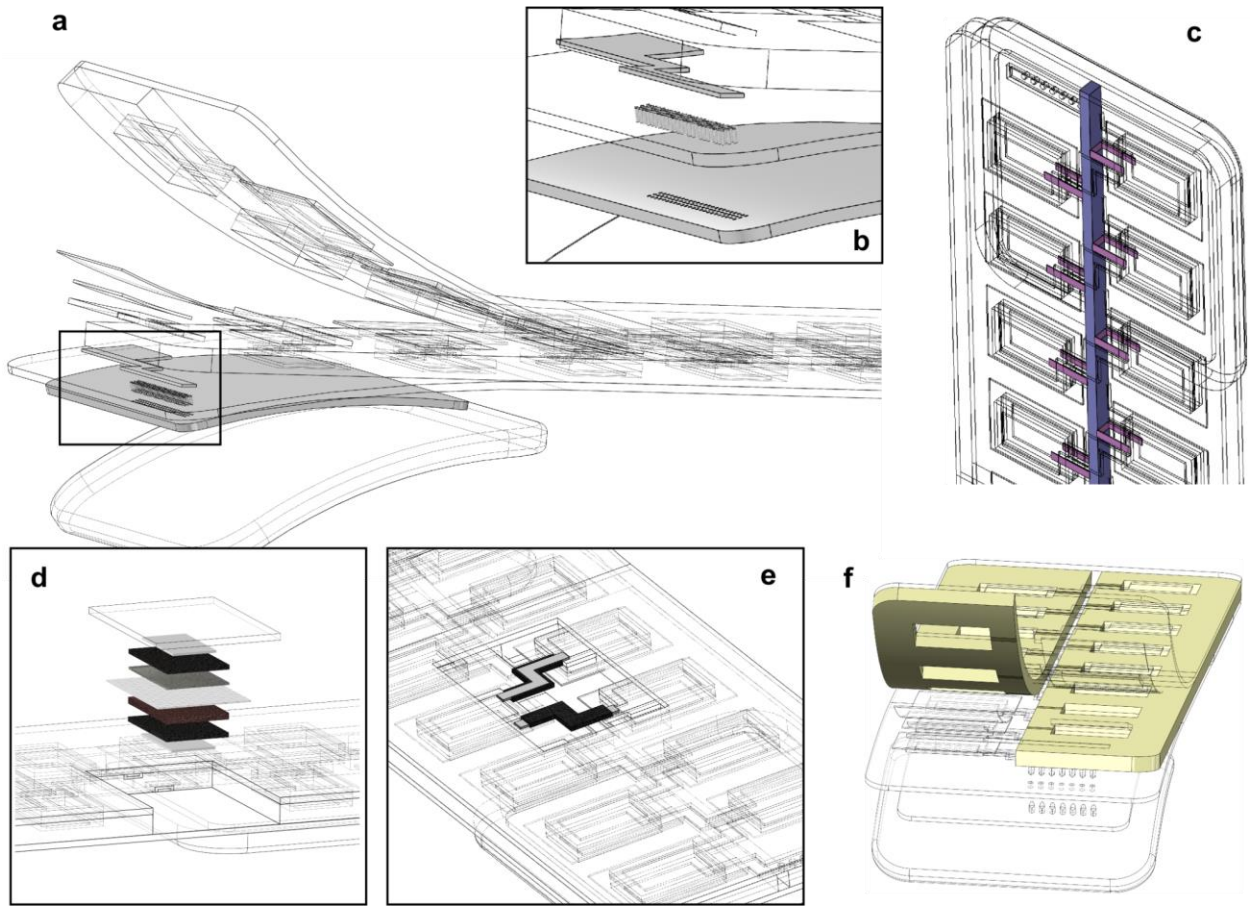

Supplementary Fig. 3. 3D Geometry of Wearable Disposable Electrotherapy device. a) Exploded view of device with **b)** Inset showing array of holes on the substrate filled with conductive material, connecting stimulation electrode on back of the substrate to the interconnect on the top of the substrate. **c)** Areal geometry showing the venting system. The vent channel (negative space) is shown in blue and normally closed valves are shown in purple. **d)** Exploded view of layers of one battery cell (top to bottom: substrate enclosure, silver conductor, carbon current collector, anode, separator, cathode, carbon current collector, silver conductor. **e)** View of two interconnects (one on bottom and one on top substrates) connecting one battery cell to two adjacent cells. **f)** Two strips of double sided tape with cutouts for battery cells, and narrow strips of adhesive masking. The 1 mm gap between adhesives forms the vent channel.

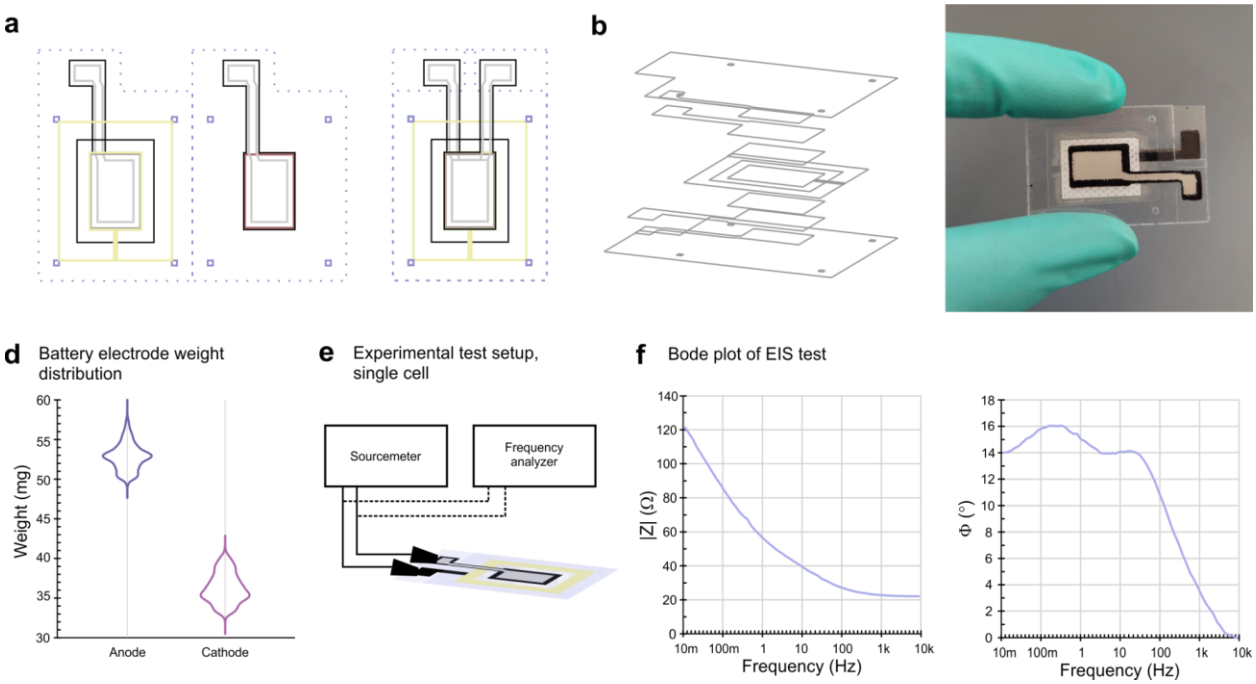

Supplementary Fig. 4. Single cell pack design and verification. a) Design of single cell for battery electrochemical testing. **b)** Exploded view of layers of single cell test device. **c)** Photograph of a single cell test device. **d)** Battery electrode weight distribution for a cell (n = 120). **e)** Experimental test setup for a single cell test device. **f)** Bode plot of electrochemical impedance spectroscopy performed potentiostatically at open circuit voltage with a small signal stimulus of 5 mV across 10 mHz - 10 kHz frequency range.

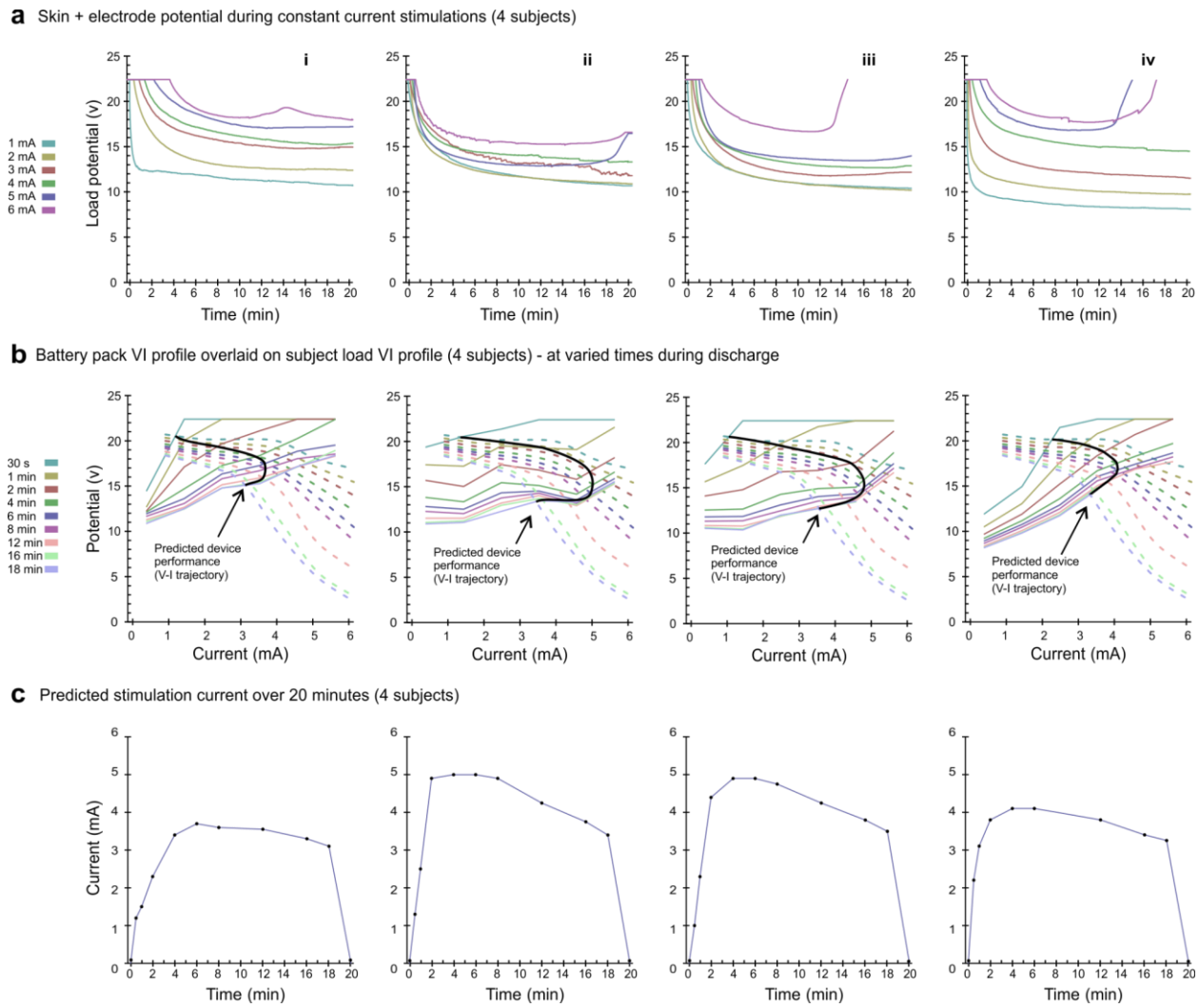

Supplementary Figure 5. Simulation of Wearable Disposable Electrotherapy device performance. a) Load test results for 4 subjects under constant current stimulation at amplitudes of 1-6 mA and voltage limit of 22.4 v during 20 minutes. **b)** The associated isotemporal V-I profile of load results (colored solid lines) are overlaid with battery pack V-I performance (colored dashed lines). Battery pack data is from galvanostatic discharge tests (1-6 mA, 20 minutes). The load and battery pack V-I profiles are at varied time points during discharge (colors). At each timepoint, the intersection of these V-I plots reflects load-matching. The connection of these intersections (solid black line) is the simulated device discharge trajectory. **c)** The predicted discharge trajectory is shown as current over time performance, with each subject's simulation with device specifications. This novel design / simulation approach was developed for Wearable Disposable Electrotherapy devices, and is then validated.

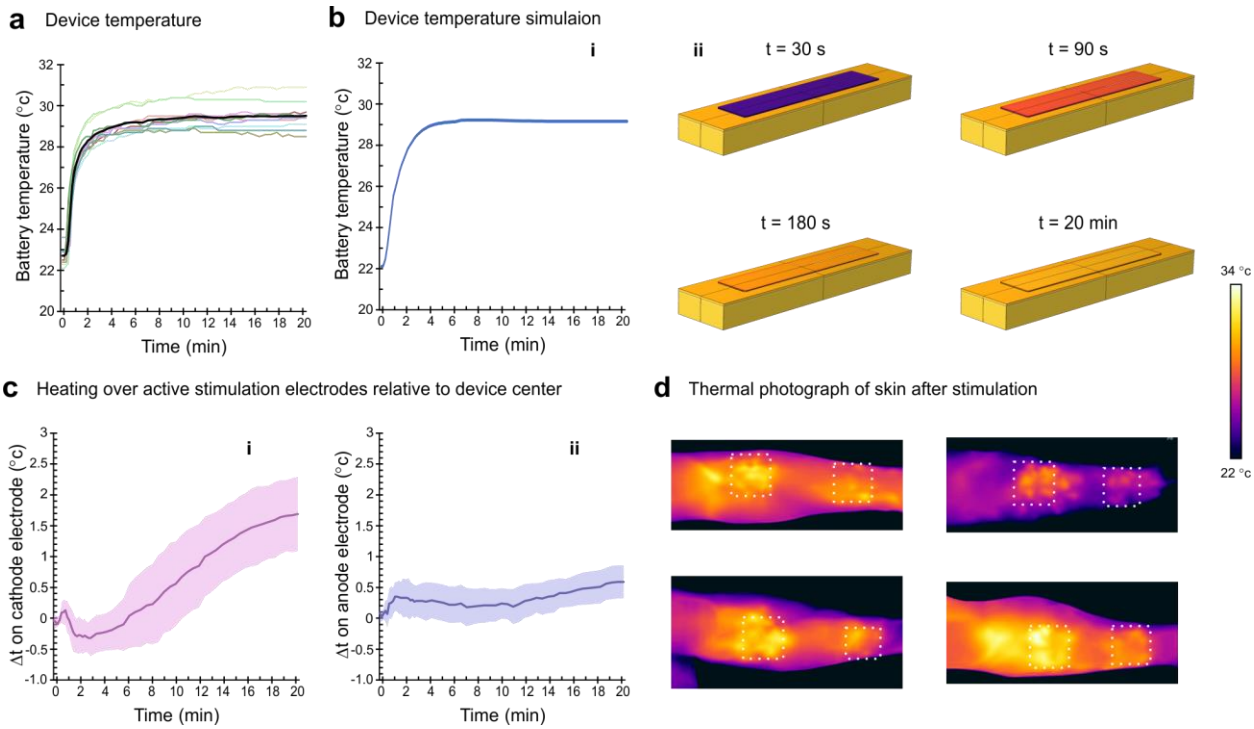

Supplementary Figure 6. Temperature Transition of Wearable Disposable Electrotherapy Device. Device temperature quickly warms to skin temperature by placement on subjects' skin (t=0). **a)** Battery pack temperature measured using sensors in place of battery active material in surrogate test devices for 10 subjects (colored lines) and average (black line). **b)** FEM bioheat simulation of battery pack temperature. **c)** Relative heating of battery material over stimulation cathode electrode (i) and over stimulation anode electrode (ii), normalized to temperature in the center of device (solid lines: average; shaded areas: variance). **d)** IR thermography of skin after stimulation showing relative heating of skin under cathode (left) and anode (right) stimulation electrodes.